Impurity effects in two-electron coupled quantum dots: entanglement modulation

Impurity effects in two-electron coupled quantum dots: entanglement modulation

Diego S Acosta Coden, Rodolfo H Romero, Alejandro Ferrón and Sergio S Gomez

Instituto de Modelado e Innovación Tecnológica (CONICET-UNNE) and Facultad de Ciencias Exactas y Naturales y Agrimensura, Universidad Nacional del Nordeste, Avenida Libertad 5400, W3404AAS Corrientes, Argentina

E-mail: aferron@conicet.gov.ar

Abstract

We present a detailed analysis of the electronic and optical properties of two-electron quantum dots with a two-dimensional Gaussian confinement potential. We study the effects of Coulomb impurities and the possibility of manipulating the entanglement of the electrons by controlling the confinement potential parameters. The degree of entanglement becomes highly modulated by both the location and charge screening of the impurity atom, resulting in two regimes: one of low entanglement and the other of high entanglement, with both of them mainly determined by the magnitude of the charge. It is shown that the magnitude of the oscillator strength of the system could provide an indication of the presence and characteristics of impurities and, therefore, the degree of entanglement.

(Some figures may appear in colour only in the online journal)

1. Introduction

Semiconductor quantum dots (QDs) are excellent candidates for realizing qubits for quantum information processing because of the potential for excellent manipulability and scalability. In contrast to real atoms and molecules, in QDs the electronic and optical properties are highly tunable. Tremendous advances in semiconductor technology allow the preparation of complex structures and give the possibility to the experimentalists to have a great control on the parameters that define the electrical and optical properties of these systems [1].

It is known that the presence of impurity centres has a great influence on the optical and electronic properties of nanostructured materials. Since the pioneering work of Bastard [2] many authors have investigated the effects of impurities on different properties of artificial atoms and molecules. A recent work [3] studied the effects of having unintentional charged impurities in two-electron laterally coupled two-dimensional double QD systems. They analysed the effects of quenched random-charged impurities on the singlet–triplet exchange coupling in two-electron double QDs. Although there is an enormous interest in applying these systems in quantum information technologies, there are few works trying to quantify the effect of charged impurities on this kind of task. The existence of unintentional impurities, which are always present in nanostructured devices, seriously affects the possibility of using these devices as quantum bits. Although the distribution and concentration of impurities in these systems result in unknown parameters, there are some recent works that propose the possibility to experimentally control these issues [9–11]. Impurity doping in semiconductor materials is considered as a useful technology that has been exploited to control optical and electronic properties in different nanodevices.

It is worth mentioning that, due to environmental perturbations, these systems lose coherence. For example, confined electrons interact with spin nuclei through the hyperfine interaction leading, inevitably, to decoherence [12]. Even having just one charged impurity could induce qubit decoherence if this impurity is dynamic and has a fluctuation time scale comparable to gate operation time scales [3]. Decoherence is a phenomenon that plays a central role in quantum information and its technological applications [13–19].

Entanglement, which is one of the most curious phenomena in quantum mechanics, is being considered in recent years as a physical resource that can be used for

quantum information processes as teleportation of quantum states [20–22]. There exists the possibility of manipulating the amount of entanglement in a QD molecule by controlling the nanostructure parameters that define the nanodevice. He and Zunger [23] studied the effect of interdot distance and asymmetry on the spatial entanglement of two-electron coupled QDs. They showed that the asymmetry in these systems significantly lowers the degree of entanglement of the two electrons. Two-electron entanglement of different QD atoms and molecules have been studied by several authors in the last decade [22–32]. The presence of nearby charged impurities, as Das Sarma and Nguyen show, have an important effect on the singlet–triplet coupling, with unwanted impact in quantum information tasks. One of the main goals of this paper is the calculation of the spatial entanglement [22, 25, 27] of the two electrons in a double QD molecule in the presence of charged impurities. Experimentally, it is very difficult to measure the amount of entanglement of two electrons in a coupled QD directly. Several techniques exist that allows one to measure the possibility of double occupation [23] and the optical properties such as the dipole transition, the oscillator strength and the photoionization cross section [33–38] of these systems. If we know the relationship between these quantities and the degree of entanglement, we can obtain information about the amount of entanglement in our system. The possibility of using this information in order to design nanodevices according to the level of entanglement desired is, as a result, quite difficult because the positions and the strength of the impurities are unknown. Despite this, there are some recent experiments which show the mechanism of dopant incorporation and how the incorporation of impurity defects can be controlled [9, 10, 39].

The aim of this work is to present a detailed analysis of the electronic and optical properties of a two-dimensional two-electron coupled QD and the effect of impurities. In particular, we show that the entanglement of the electrons is strongly modulated by the position and charge of the impurity. We also show that optical measurements would allow information about the effect of the impurity in these kinds of devices to be obtained. This paper is organized as follows. In section 2, we introduce the model for the two-dimensional two-electron coupled QD and briefly describe the method used to calculate its electronic structure. In section 3, we calculate the spatial entanglement in the presence of one impurity and discuss its relation to the exchange coupling. Section 4 contains calculations of the oscillator strength for a range of parameters of the system that show the modifications of the optical properties in the presence of a charged impurity, with the aim of allowing optical measurements to be correlated with the degree of entanglement of the system. Finally, in section 5 we summarize the conclusions with a discussion of the most relevant points of our analysis.

2. The model and calculation method

We consider two laterally coupled two-dimensional QDs whose centres are separated a distance d from each other, and contain two electrons. In QDs electrostatically produced, both their size and separation can be controlled by variable gate voltages through metallic electrodes deposited on the heterostructure interface. The eventual existence of doping hydrogenic impurities, probably arising from Si dopant atoms in the GaAs quantum well, have been experimentally studied [4]. These impurities have been theoretically analysed with a superimposed attractive $1/r$-type potential [5, 6]. Furthermore, some avoided crossing and lifted degeneracies in the spectra of single-electron transport experiments have been attributed to negatively charged Coulomb impurities located near to the QD [7]. From fitting the experimental transport spectra to a single-electron model of softened parabolic confinement with a Coulomb charge q, a set of parameters are obtained; among them, a radius of confinement of 15.5 nm, a confinement frequency $\hbar\omega = 13.8$ meV and an impurity charge of approximately 1 or 2 electron charges. Indeed, the uncertainty in the parameters and the suppositions introduced in the model does not allow one to precisely ensure the impurity charge, with the screening probably reducing its effective value to less than an electron charge. Therefore, we consider the charge of the doping atom Ze as a parameter varying in the range $0 \leqslant Z \leqslant 1$, in order to explore its effect on the properties of the system.

In this work we model the Hamiltonian of the two-dimensional two-electron coupled QD in the presence of charged impurities within the single-conduction-band effective-mass approximation [8], namely,

$$H = h(\mathbf{r}_1) + h(\mathbf{r}_2) + \frac{e^2}{4\pi\varepsilon\varepsilon_0 r_{12}}, \tag{1}$$

where $\mathbf{r}_i = (x_i, y_i)$ $(i = 1, 2)$ and

$$h(\mathbf{r}) = -\frac{\hbar^2}{2m^*}\nabla^2 + V_L(\mathbf{r}) + V_R(\mathbf{r}) + V_A(\mathbf{r}), \tag{2}$$

where $h(\mathbf{r})$ is the single-electron Hamiltonian that includes the kinetic energy of the electrons, in terms of their effective mass m^*, and the confining potential for the left and right QDs V_L and V_R, and the interaction of the electrons with the charged impurities, V_A.

The last term of the Hamiltonian, equation (1), represents the Coulomb repulsive interaction between both electrons at a distance $r_{12} = |\mathbf{r}_2 - \mathbf{r}_1|$ apart from each other, within a material of effective dielectric constant ε. We model the confinement with Gaussian attractive potentials

$$V_i(\mathbf{r}) = -V_0 \exp\left(-\frac{1}{2a^2}|\mathbf{r} - \mathbf{R}_i|^2\right), \quad (i = L, R), \tag{3}$$

where $\mathbf{R}_L$ and $\mathbf{R}_R$ are the positions of the centre of the left and right dots, V_0 denotes the depth of the potential and a can be taken as a measure of its range. Along this work, we will consider a single impurity atom centred at $\mathbf{R}_A$, and modelled as a hydrogenic two-dimensional Coulomb potential

$$V_A(\mathbf{r}) = -\frac{Ze^2}{4\pi\varepsilon\varepsilon_0|\mathbf{R}_A - \mathbf{r}|}. \tag{4}$$

Since the Hamiltonian does not depend on the electron spin, its eigenstates can be factored out as a product of a spatial and a spin part

$$\Psi_i(\mathbf{r}_1, \mathbf{r}_2, m_{s_1}, m_{s_2}) = \Psi_i^S(\mathbf{r}_1, \mathbf{r}_2)\chi_{S,M}, \tag{5}$$

where $S = 0, 1$ for singlet and triplet states, respectively, and $M = m_{s_1} + m_{s_2}$ is the total spin projection.

The eigenstates of the model Hamiltonian can be obtained by direct diagonalization in a finite basis set [40]. The spatial part is obtained, in a full configuration interaction (CI) calculation, as

$$\Psi_m^S(\mathbf{r}_1, \mathbf{r}_2) = \sum_{n=1}^{N_{conf}} c_{mn}^S \Phi_n^S(\mathbf{r}_1, \mathbf{r}_2) \qquad (6)$$

where N_{conf} is the number of singlet ($S = 0$) or triplet ($S = 1$) two-electron configurations $\Phi_n^S(\mathbf{r}_1, \mathbf{r}_2)$ considered, and $n = (i, j)$ is a configuration label obtained from the indices i and j from a single electron basis, i.e.

$$\Phi_n^S(\mathbf{r}_1, \mathbf{r}_2) = \tfrac{1}{\sqrt{2}} [\phi_i(\mathbf{r}_1)\phi_j(\mathbf{r}_2) + (1 - 2S)\phi_j(\mathbf{r}_1)\phi_i(\mathbf{r}_2)] \quad (7)$$

for $i \neq j$, and $\Phi_n^{S=0}(\mathbf{r}_1, \mathbf{r}_2) = \phi_i(\mathbf{r}_1)\phi_i(\mathbf{r}_2)$ for the doubly occupied singlet states.

We chose a single-particle basis of Gaussian functions, centred at the dots and atom positions $\mathbf{R}_P$ ($P = L, R, A$), of the type [41, 42]

$$\phi_i(\mathbf{r}) = N x^{m_i} y^{n_i} \exp(-\alpha_i |\mathbf{r} - \mathbf{R}_P|^2), \qquad (8)$$

where N is a normalization constant, and $\ell_i = m_i + n_i$ is the z-projection of the angular momentum of the basis function. The exponents α_i were optimized for a single Gaussian well and a single atom separately, and supplemented with extra functions when used together. For our calculations a basis set of 2s2p functions for the dots, and 5s5p1d1f for the atom was found to achieve converged results for the energy spectrum.

The numerical results presented in this work refers to those corresponding to the parameters of GaAs: effective mass $m^* = 0.067m_e$, effective dielectric constant $\varepsilon = 13.1$, Bohr radius $a_B^* = 10$ nm and effective atomic unit of energy 1 Hartree$^* = 10.6$ meV [7, 3]. The depth of the Gaussian potentials modelling the dots are taken as $V_0 = 4$ Hartree$^* = 40.24$ meV, and its typical range $a = \sqrt{2}a_B^* = 14.1$ nm.

3. Entanglement entropy and exchange coupling

The proposed applications of QDs for quantum computing require a large exchange coupling between electrons along separated regions of space. To some extent, both requirements compete with each other. In a simple picture, one could have a large exchange coupling for electrons doubly occupying the same dot or atom. In such a case, the singlet state has the form of a product wave function $\varphi_0(\mathbf{r}_1)\varphi_0(\mathbf{r}_2)$ with the corresponding singlet spin function; the lowest triplet state, however, has the form of the antisymmetrized product of two single-electron functions, $\varphi_0(\mathbf{r}_1)\varphi_1(\mathbf{r}_2) - \varphi_0(\mathbf{r}_2)\varphi_1(\mathbf{r}_1)$, of different single-particle energies ε_0 and ε_1. Thus, the triplet state will have a quite higher energy than the singlet state, thus giving a large exchange coupling. Nevertheless, such a large coupling is not favourable for quantum computing tasks because the states are localized in space. Using electron states as qubits requires, for instance, the feasibility to detect the single or double occupancy of two QDs, separated a measurable distance, while keeping both electrons correlated.

As the interdot separation increases, the electron–electron interaction diminishes and its relative importance with respect to the confining potential tends to vanish. In the limit of
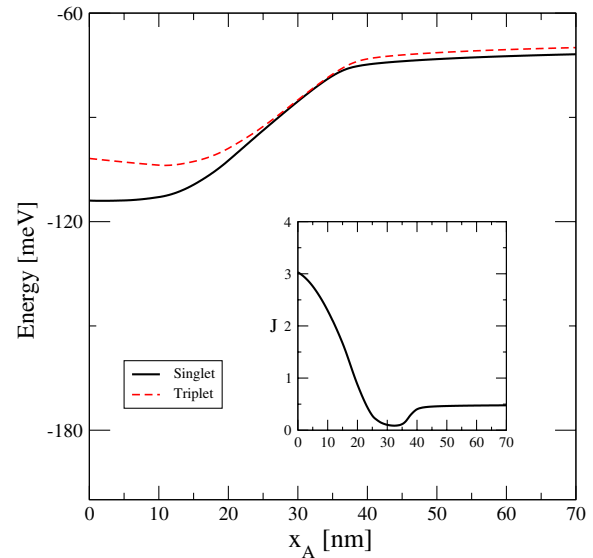

Figure 1. Calculated ground-state energy of the two-electron double QD, for an interdot distance $d = 30$ nm, with one impurity atom of charge $Z = 1$ located along the interdot axis as a function of impurity position. The black line (red dashed line) shows the singlet (triplet) ground-state energy. The inset shows the singlet–triplet exchange coupling J as a function of impurity position.

large interdot separations, the Coulomb repulsion is minimized by singly occupying each of the QDs with an electron. In such a limit, the energies of both the singlet ($+$) and triplet ($-$) states, $\varphi_0(\mathbf{r}_1)\varphi_1(\mathbf{r}_2) \pm \varphi_0(\mathbf{r}_2)\varphi_1(\mathbf{r}_1)$ approach the sum of singly occupied dots and their difference J tends to zero. In other words, the best conditions for applications to quantum information processing arises from a compromise between a high spatial correlation of pairs of electrons at the longest possible lengths where the exchange coupling J is still sizable. This behaviour is illustrated in figure 1, assuming a positively charged impurity of one electron charge ($Z = 1$).

Figure 1 shows the singlet and triplet ground-state energies for the double QD, separated a distance $d = 30$ nm, as a function of impurity position x_A. The inset shows the behaviour of the singlet–triplet exchange coupling as a function of the impurity position. These results are in qualitative agreement with those of [3]. The singlet–triplet exchange coupling is strongly affected for the presence of the charged impurity, it has the maximum value when the impurity is centred in between the two dots, and it has a minimum close to zero when the impurity is located at $x_A = d$. Expectedly, the splitting goes asymptotically to the impurity-free double QD case when the impurity atom is located far away from the double QD system. We shall show below that the impurity positions that give high energy splitting, i.e. those near to the middle of the interdot distance, correspond to a two-electron ground state whose spatial wave function is highly localized at the impurity atom, thus having a small spatial entanglement.

In what follows we shall restrict ourselves to the impurity located along the interdot x-axis, $\mathbf{R}_A = (x_A, 0)$.

We shall study now how the degree of spatial quantum correlation of two electrons in the coupled QD is modified by the position and charge of a screened atomic impurity.
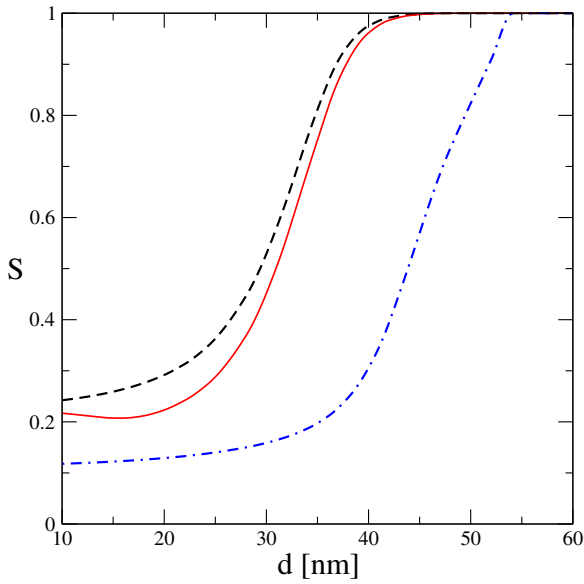
Figure 2. von Neumann entropy of the reduced density matrix for the two-electron coupled QD as a function of the interdot distance. The black dashed line shows the entropy when there is no impurity present in the sample, the red line corresponds to the entropy when a single impurity $Z = 0.1$ is located at $x = y = 0$ and the blue dotted–dashed line corresponds to $Z = 1.0$.

As mentioned above, the eigenstate wave functions can be factorized in its orbital and spin part. For the ground state, the spin part is a singlet wave function, which is maximally entangled and constant. Therefore, throughout this work, we will only consider the spatial entanglement [22, 25, 27–29].

The von Neumann entropy of the reduced density matrix quantifies the entanglement for a bipartite pure state and can be calculated using [25, 27–30]

$$S = -\mathrm{Tr}(\hat{\rho}^{\mathrm{red}} \log_2 \hat{\rho}^{\mathrm{red}}), \qquad (9)$$

where $\hat{\rho}^{\mathrm{red}} = \mathrm{Tr}_2 |\Psi\rangle\langle\Psi|$ is the reduced density operator, Ψ is the two-electron wave function and the trace is taken over one electron. The von Neumann entropy could be written as

$$S = -\sum_i \lambda_i \log_2 \lambda_i, \qquad (10)$$

where λ_i are the eigenvalues of the spatial part of the reduced density operator

$$\int \rho^{\mathrm{red}}(\mathbf{r}_1, \mathbf{r}_1')\phi_i(\mathbf{r}_1')\,\mathrm{d}\mathbf{r}_1' = \lambda_i \phi_i(\mathbf{r}_1), \qquad (11)$$

where

$$\rho^{\mathrm{red}}(\mathbf{r}_1, \mathbf{r}_1') = \int \Psi^*(\mathbf{r}_1, \mathbf{r}_2)\Psi(\mathbf{r}_1', \mathbf{r}_2)\,\mathrm{d}\mathbf{r}_2. \qquad (12)$$

Figure 2 shows the von Neumann entropy for two electrons in the double QD as a function of its interdot distance, in the absence of impurity (black dashed line) and with atomic charges $Z = 1$ (blue dashed–dotted line) and $Z = 0.1$ (red solid line) located at the centre of the double QD. In all of the cases it is observed that, for small interdot separations, the entropy is small, smoothly increasing with the interdot separation. The increase of the spatial entanglement is due to a gradual delocalization of the ground state wave function. For interdot distances between 20 and 40 nm, there is a large increase of
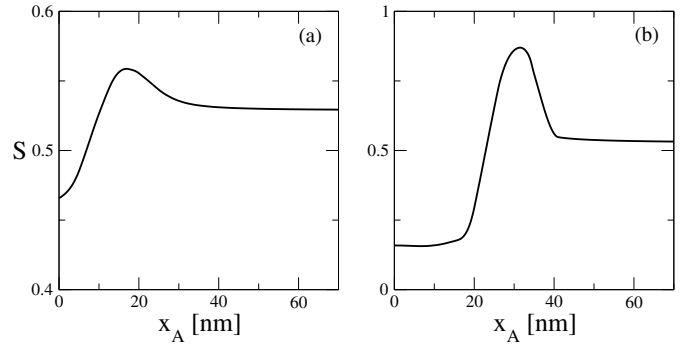

Figure 3. von Neumann entropy of the reduced density matrix for the two-electron coupled QD as a function of the impurity position (along the interdot axis) for $d = 30$ nm and different impurities strengths: (a) $Z = 0.1$ and (b) $Z = 1.0$.

the entanglement entropy, signalling a qualitative change of the ground state wave function from an atomic doubly occupied state to a state with both dots singly occupied, reached at large interdot separations ($d \gtrsim 50$ nm), where the entropy saturates to its maximum $S = 1$. The variation of S is similar for all of the cases, although the presence of the impurity decreases the entanglement for every interdot separation, due to the fact that the atomic potential contributes to the localization of the electronic density at the centre of the system.

The effect of the charge and location of the impurity on the spatial entanglement, for fixed QDs geometry, can be observed in figure 3, where the entropy is depicted as a function of the impurity position. The separation between the two QDs is kept fixed at 30 nm, and two limiting cases are considered: a highly screened atomic charge $Z = 0.1$ and an unscreened charge $Z = 1$. In both cases, the entanglement entropy increases as the impurity moves off the centre of the double QD until a position where S reaches a maximum, finally decreasing to a value $S = 0.53$, when the atom is distant from the dots ($x \gtrsim 40$ nm).

The minimum and maximum of entanglement produced by the small charge $Z = 0.1$ are less pronounced than those due to the highly charged impurity $Z = 1$. This modulation of the entanglement by the impurity position reflects the existence of two regimes: one of low entanglement for impurities at (or near to) the centre of the interdot distance, and another of higher (but not maximum) entanglement for atomic positions external to the interdot segment. In figure 3, these two regions are the ones to the left and the right of the bell-shaped peak of S, respectively. The peak position itself depends on the magnitude of the charge. For small charges, the maximum degree of entanglement occurs at $x_A \approx 17$ nm, that is, close to the centre of the dot to the right. For the large charge $Z = 1$, however, the peak of S occurs at $x \approx 30$ nm. The rationale for it is that, for low charged impurities, the atomic potential is a weak perturbation to the QDs potential wells. Therefore, the entropy varies in a small range ($0.47 \leqslant S \leqslant 0.56$) around the impurity-free case $S = 0.53$. For large impurity charges, nevertheless, the atomic potential is strong and the position of its centre greatly determines the spatial wave function. The range of atomic positions ($0 \leqslant x_A \lesssim 20$ nm) along which S remains low, can be understood to be due to the localization of
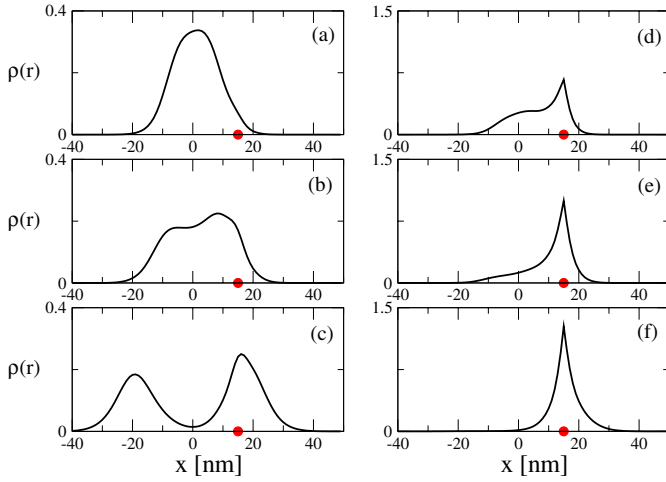
Figure 4. Ground state one-electron density along the interdot axis. Left panels show the weak impurity limit $Z = 0.2$ and right panels the strong impurity limit $Z = 0.8$: (a) and (d) $d = 15$ nm, (b) and (e) $d = 25$ nm and (c) and (f) $d = 40$ nm. Red circles show the impurity position $x_A = 15$ nm.
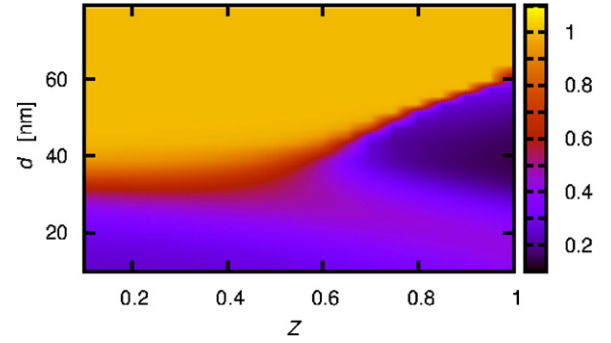

Figure 5. Contour map for the von Neumann entropy of the reduced density matrix for the two-electron coupled QD as a function of impurity strength and interdot distance for $x_A = 15$ nm.
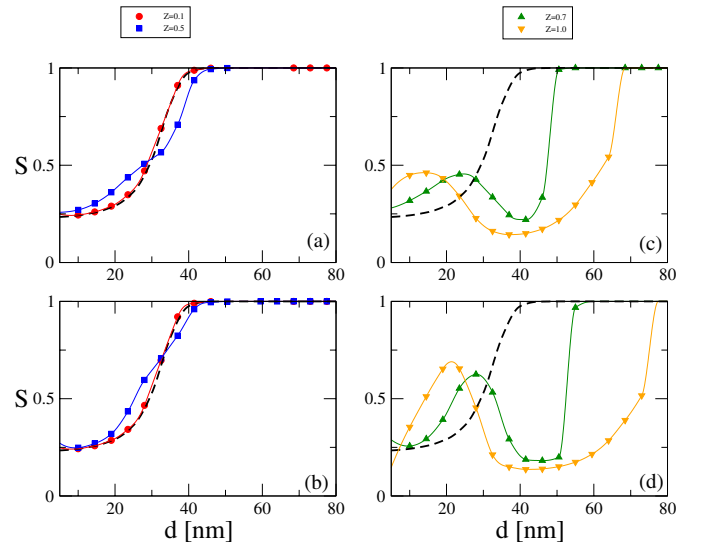

Figure 6. von Neumann entropy of the reduced density matrix for the two-electron coupled QD as a function of the interdot distance for $x_A = 15$ nm ((a) and (c)), $x = 20$ nm ((b) and (d)) and different values of the impurity strength. (a) and (b) The weak impurity limit ($Z = 0.1$ and $Z = 0.5$) while in (c) and (d) we observe the strong impurity limit ($Z = 0.7$ and $Z = 1.0$). The black dashed line shows the behaviour of the entropy when there are no impurities in the sample.

the electrons close to the atom. When the atom is inside one of the dots (QD_R), the atomic potential reinforces that of the dot well and the electron density localization, thus giving a low degree of entanglement. When the atom moves towards outside the double QD, the strength of the double well competes with the large atomic potential until an atom-double QD distance of about 30 nm, where it becomes energetically convenient to delocalize the electron wave function, resembling the double QD bond in the absence of impurity.

To show the influence of the atomic charge on the wave function clearly, let us consider two slightly less extreme situations: $Z = 0.2$ and $Z = 0.8$. Figure 4 shows the ground state electron density along the interdot axis when the impurity atom is located at $x_A = 15$ nm, for three different interdot separations, $d = 15$, 25 and 40 nm. The panels to the left show that for the small charge, as the QDs separate from one another, the electron density develops peaks located at the potential well centres. For the large charge $Z = 0.8$, however, the density is always peaked at the impurity position. Therefore, in this last case, the presence of the impurity could spoil the performance of the device for quantum computing tasks due to the fact that the high localization of the electron density entails a low degree of entanglement.

Figure 5 shows the dependence of the von Neumann entropy on the impurity charge and interdot distance for a given position of the impurity atom: $x_A = 15$ nm. Ideally, provided that the value of the impurity charge could be measured in a given sample, one would be able to choose the optimal interdot distance for a given degree of entanglement. The figure clearly shows the aforementioned regimes of weak ($Z \lesssim 0.6$) and strong ($Z \gtrsim 0.6$) impurity potentials, corresponding to a low and high degree of entanglement, respectively. For a given (fixed) small impurity charge Z, the entropy increases monotonically as the interdot distance d increases. On the other hand, for a given large Z, by increasing the distance d, the entropy increases for small distances d up to a maximum

value, diminishes to a minimum and sharply increases again until its asymptotic impurity-free value $S = 1$.

Figure 6 shows the dependence of the entropy on the interdot distance, for different impurity positions ($x_A = 15$ and 20 nm) and charges ($Z = 0.1$, 0.5, 0.7 and 1). The corresponding variation in the absence of impurity is also represented by dashed lines for reference. Two qualitatively distinct behaviours for small ($Z = 0.1$, 0.5) and large ($Z = 0.7$, 1) charges can be seen. The monotonic increase of S with d is characteristic of the weak atomic potential; separating the QDs with a small atomic charge between them, produces little changes in the electron distribution as compared with the impurity-free double QD. On the other hand, strong atomic potentials induce a modulation of the entropy as d increases; for small values of d, all three potentials are close to each other and the electron density localizes around their centres. For large interdot distances, the energy of the system is minimized
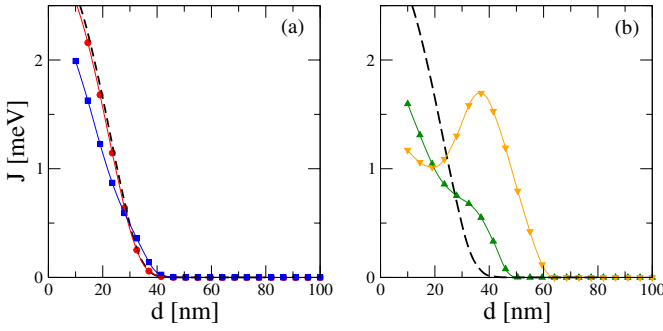
Figure 7. *J* as a function of the interdot distance *d* with an impurity centre located at $x_A = 15$ nm. On the left panel (a) we observe the singlet–triplet coupling for $Z = 0.1$ (red circles) and $Z = 0.5$ (blue squares). In (b) we show the singlet–triplet coupling for $Z = 0.7$ (green up triangles) and $Z = 1.0$ (orange down triangles). The black dashed line represents the singlet–triplet with no impurity.

by decreasing the electronic repulsion, i.e. by delocalizing the wave function and, hence, increasing its entanglement.

Figure 7 shows this effect on the exchange coupling corresponding to situations of figures 6(a) and (c), having the atom at $x_A = 15$ nm. It can be observed that *S* and *J* have, roughly, opposite variations; whence the atomic potential is weak, *S* increases and *J* decreases as the QDs separate from each other. In the regime when the atomic potential is strong, the maximum of *S* occurs at the minimum of *J* and reciprocally; furthermore, at large QD separations, as the entropy goes to its asymptotical value $S = 1$, the exchange coupling tends to zero. Then, for specific quantum information applications, it could be desirable to tune the interdot distance for harnessing one or both properties.

The variety of behaviours of the degree of spatial entanglement with the various parameters of the system, described in this section, is rooted in the spatial distribution of the electron wave function. We shall discuss in the next section a relation with an optical property, like the oscillator strength, in order to provide a feasible connection with measurable magnitudes.

4. Impurity effect on the optical properties

The optical susceptibility of a system depends on its transition amplitude for the interaction of its dipole moment with the optical electric field between two singlet states Ψ_i and Ψ_j, say the ground and excited states, and the corresponding energy differences. The oscillator strength for an electric field applied along the interdot axis

$$f_{ij} = \frac{2m^*}{\hbar}(E_j - E_i)|\langle\Psi_i|x_1 + x_2|\Psi_j\rangle|^2, \quad (13)$$

takes both magnitudes into account and provides information on the feasibility of such optical excitations.

We study here how the impurity affects the oscillator strength of the double QD. The dots are kept 30 nm separated from each other and the position of the impurity x_A is varied from the centre of the interdot segment ($x_A = 0$) to a large separation from the dots ($x_A = 70$ nm), including the case of the impurity centred in one dot ($x_A = 15$ nm). The charge *Z*
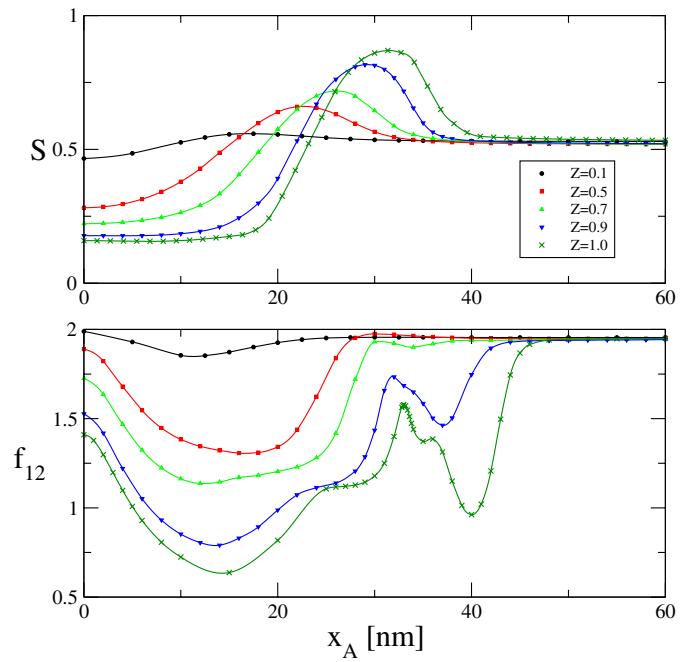

Figure 8. von Neumann entropy of the reduced density matrix (upper panel) and oscillator strength f_{12} (lower panel) between the ground and first excited singlet state of a double QD with an impurity of charge *Z* as a function of the impurity position x_A, for different values of *Z*.

of the atom is varied from $Z = 0.1$ (highly screened impurity) to $Z = 1$ (low screening). For the system considered, the oscillator strength between the ground and the first excited singlet states, f_{12}, is the dominant contribution with respect to all others f_{ij}. The precision of the calculation was checked by verifying the Thomas–Reiche–Kuhn sum rule, $\sum_{ij} f_{ij} = N$, with $N = 2$ being the number of electrons in the system. The results are shown in figure 8 together with the entanglement entropy for the same atomic positions and charges.

The cases of weak and strong electron–atom Coulomb interaction are clearly distinguishable. In the regime of small impurity charge ($Z \lesssim 0.6$), the oscillator strength f_{12} varies approximately with a quadratic dependence on x_A; i.e. it starts from $f_{12} \approx 2$, reaches a minimum around $x_A = 15$ nm, and finally increases up to a value of 2, at nearly $x_A = 30$ nm. The larger the impurity charge *Z*, the more pronounced the minimum of f_{12}. Placing the atom further away from the double dot system ($x_A > 30$ nm) does not change f_{12}.

On the other hand, in the regime of high impurity charge ($Z \gtrsim 0.6$), the oscillator strength f_{12} exhibits richer features as compared to the small charge case. The most remarkable behaviour corresponds to $Z = 1$ which successively shows a similar decreasing, from $f_{12} = 1.4$ at $x_A = 0$, to $f_{12} = 0.6$ at $x_A = 15$ nm, followed by an increase up to $x_A = 25$ nm, a small plateau around 30 nm, a peak at $x_A = 33$ nm, a minimum of $f_{12} \approx 1$ at 40 nm, finally approaching the saturation value $f_{12} = 2$ for $x_A \gtrsim 50$ nm. For intermediate $0.5 \leqslant Z \leqslant 1$ values, a gradual transition between both regimes is observed; namely, by decreasing *Z* from 1 to 0.5, the minimum of the region $x_A \approx 40$ nm becomes shallower, the peak is softened, and the plateau merges with the minimum occurring at 15 nm, thus giving the flat minimum of the weak impurity regime.
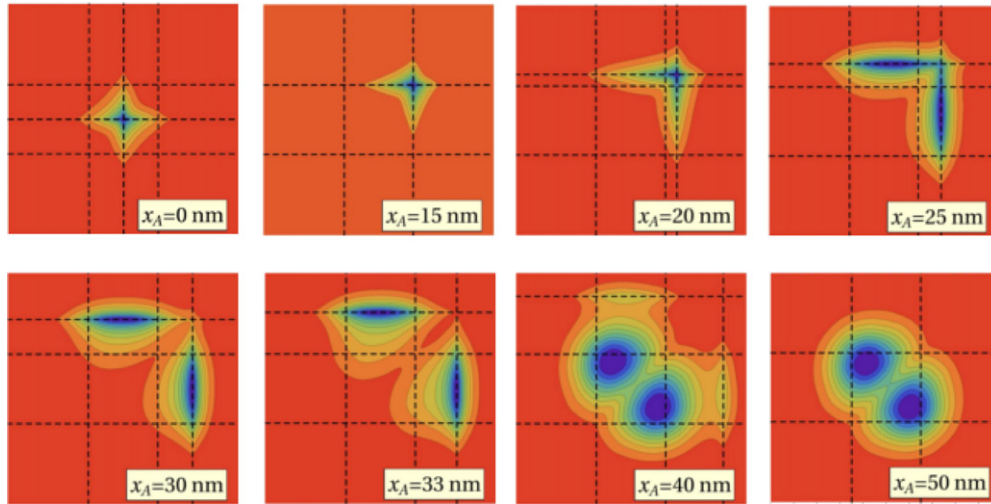
Figure 9. Contour plot in the (x_1, x_2)-plane of the two-electron ground state singlet wave function, $\Psi_1(x_1, x_2)$, along the interdot axis x for the ground state of the doped double QD. Gaussian wells are centred at $\mathbf{R}_L = (x_L, 0)$ and $\mathbf{R}_R = (x_R, 0)$ and the impurity atom of charge $Z = 1$, at $\mathbf{R}_A = (x_A, 0)$. The vertical and horizontal dashed lines $x_i = x_L, x_R$ or x_A ($i = 1, 2$), signals the condition where one electron (electron 1 or 2, respectively), is at the centre of the dot to the left, to the right or at the impurity atom. The centres of the dots $x_R = -x_L = 15$ nm are held symmetrical with respect to the origin of coordinates. The atom is successively placed at $x_A = 0, 15, 20, 25, 30, 33, 40$ and 50 nm.

It should be noted that the range $0 \leqslant x \leqslant 15$ nm corresponds to an impurity atom located in between the dots, while for $x_A \geqslant 15$ nm, the atom is outside the segment defined by the interdot centres. Consequently, the existence of an impurity in the system would cause f_{12} to diminish and, therefore, the light absorption or emission of the double dot device. This effect is stronger the closer the atom is to one dot. The most favourable situation for optical excitation (high f_{12}) corresponds to an impurity centred in between the dots or outside the interdot separation, far away from any of them.

In the following we shall discuss the behaviour of the oscillator strength as being due to changes in the electronic structure induced by the variation of the position of the impurity, starting with the most striking case of a highly charged impurity $Z = 1$. We displace the atom along the line joining both dots, which we take as the x-axis; therefore, we consider the two-particle wave function along the x-axis for the coordinates x_1 and x_2 of each electron

$$\Psi_i(x_1, x_2) = \Psi_i(\mathbf{r}_1, \mathbf{r}_2) = \Psi_i(x_1, 0; x_2, 0), \qquad (14)$$

for the two lowest singlet states $\Psi_i(\mathbf{r}_1, \mathbf{r}_2)$, $i = 1$ (ground state) and $i = 2$ (first excited state). The function $\Psi_i(x_1, x_2)$, represented as a two-dimensional plot in the (x_1, x_2)-plane, allows one to visualize the most relevant configurations contributing to the total wave function. Because of the permutation symmetry, the spatial wave function satisfies $\Psi(x_1, x_2) = \Psi(x_2, x_1)$, thus becoming symmetric under reflection with respect to the diagonal $x_1 = x_2$. Large values of $\Psi(x, x)$, along this diagonal, correspond to ionic or doubly occupied configurations. In contrast, large density values $\Psi(x, -x)$ along the $x_1 = -x_2$ diagonal, corresponds to configurations where the electrons are mostly in opposite (left and right) half-planes.

In the present calculations, the x coordinates of the centres of the left and right dots $x_L = -15$ nm, $x_R = 15$ nm are

held fixed while that of the atom, $x_A = x$, varies. Large values of $\Psi(x_L, x_L)$, $\Psi(x_R, x_R)$ or $\Psi(x_A, x_A)$ entail a doubly occupied configuration at the left dot, the right dot or the atom, respectively.

On the other hand, a configuration of one electron in the atom and the other in a bond (antibond) between the left and right dots, would be represented by

$$\Psi(x_1, x_2) = [c_L\varphi_L(x_1) \pm c_R\varphi_R(x_1)]\varphi_A(x_2) + (x_1 \leftrightarrow x_2), \quad (15)$$

where the last term represents a term similar to the first one with the variables interchanged, and φ_a is a wave function centred around x_a ($a = L, R, A$). Then, $\Psi(x_1, x_2)$ will have large values close to (x_L, x_A) and (x_R, x_A) with the same or opposite sign for a bond or antibond, respectively.

Figures 9 and 10 show the plot of the ground state $\Psi_0(x_1, x_2)$ and the first singlet excited state $\Psi_1(x_1, x_2)$ from our calculations.

For a single-electron symmetric double dot system without impurity, the ground and first excited states are the bonding and antibonding states formed from the linear combination of orbitals centred at each dot. For the two-electron symmetric double dot system, figures 9 and 10 show that when the atom is at the centre of the line joining both dots ($x = 0$), the two-particle wave function of the ground state (excited state) roughly corresponds to one electron in the atom and the other in the bond (antibond) of the double dot system, equation (15). Therefore, the matrix element $\langle\Psi_0|x_1 + x_2|\Psi_1\rangle$ roughly correspond to the sum of those for the atom and the double dot separately.

At $x = 15$ nm, the atom is at the centre of the dot to the right, the system becomes very asymmetric, with the potential of the dot to the right deeper than the one to the left due to the contribution of the attractive impurity. The bond becomes a doubly occupied state localized close to the centre of the combined potential (QD$_R$ and impurity), while the
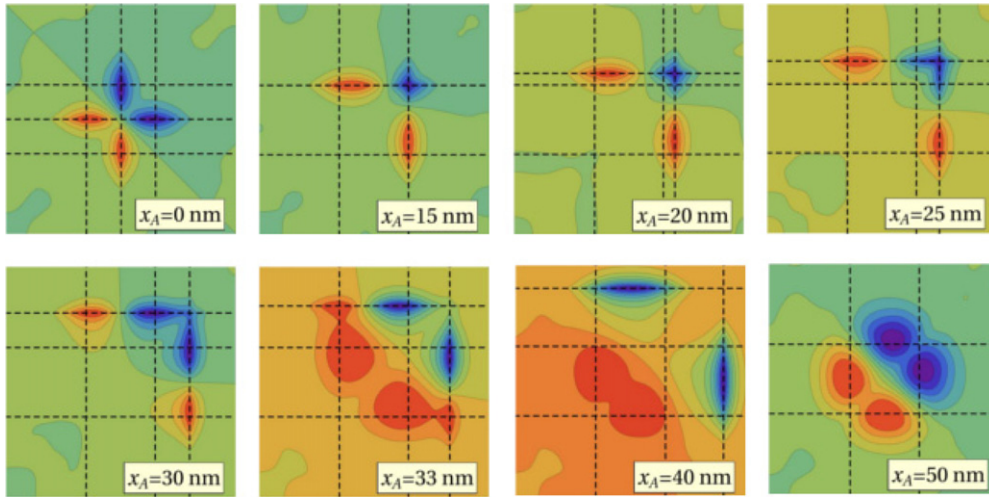
Figure 10. Same as figure 9 for the first excited two-electron singlet wave function $\Psi_2(x_1, x_2)$.

antibond becomes more localized around QD_L, due to the orthogonality condition, which lowers f_{12}. The behaviour in the range $0 \leqslant x \leqslant 15$ nm reflects this gradual change.

From 15 to 30 nm, the effect of the impurity turns weaker as the atom moves away, and the two dots become more symmetric again; this redistributes the charge towards QD_L, recovering some bonding and antibonding character for Ψ_1 and Ψ_2, respectively. Such a configuration favours an increase of f_{12}. Furthermore, as one electron remains in the atom, which is farther from the origin, the matrix element of x becomes larger than the one corresponding to the atom at the origin. The oscillator strength has a peak at 33 nm roughly increasing quadratically with the position of the atom as a consequence of the stretching of the charge.

After 33 nm, the electron in the atom cannot be retained by the impurity potential, thus Ψ_1 approaches a configuration with one electron in each dot. Nevertheless, the excited state Ψ_1 still has a configuration where the atom is occupied, which lowers f_{12}.

For atom positions further than 40 nm, the excited state also releases its electron and the double QD becomes even more symmetric, approaching its behaviour in the absence of impurity, thus approaching its value $f_{01} = 2$. The limit of isolated dots is clearly seen in figures 9 and 10, where for $x \gtrsim 50$ nm, the ground and first excited states are, approximately, $\Psi_0 \approx [\varphi_L(x_1)\varphi_R(x_2) + \varphi_R(x_1)\varphi_L(x_2)]/\sqrt{2}$ and $\Psi_1 \approx [\varphi_L(x_1)\varphi_L(x_2) - \varphi_R(x_1)\varphi_R(x_2)]/\sqrt{2}$.

As seen from figure 8, the oscillator strength for impurity charges smaller than $Z = 1$, has simpler features. Basically, they start from a value f_{12} slightly less than 2, decreases until a minimum as the atom approaches one dot, say QD_R, and increases again smoothly until reaching the asymptotic impurity-free value of 2.

The oscillator strength is a highly sensitive property to the presence of the impurity. A value of f_{12} close to 2, occurs either when the impurity is weak wherever it is located, or when a highly charged impurity atom is far away from the double QD. Both cases are situations where the impurity is a perturbation for the coupled QDs and, therefore amenable for use in quantum computing. In contrast, deviations of the

oscillator strength from a value of 2, provides an indication of a breakdown of the possibility to consider the system as a double QD.

5. Conclusions

In this work, we have studied the influence of a Coulomb atomic impurity on the entanglement entropy of two-dimensional two-electron double quantum dots. The electronic structure was calculated by using a configuration interaction method with a Gaussian basis set expansion. The degree of entanglement becomes highly modulated by both the location and charge screening of the impurity atom. Two regimes are clearly identified: one of low entanglement and the other of high entanglement, with both of them mainly determined by the magnitude of the charge. The exchange coupling between the electrons, being proportional to singlet–triplet exchange coupling, has an opposite behaviour with respect to the one of the entropy. The efficient use of double QDs with impurities, in particular quantum information processing tasks could require the tuning of the interdot separation or the quantum well depths, for optimizing the harnessing of the entanglement, the exchange coupling or both. Finally, the magnitude of the oscillator strength of the system could provide an indication of the presence and characteristics of impurities that could largely influence the degree of entanglement of the system. It is clear that experimentally obtained optical properties can help in the design of double QDs with desirable properties in order to use them in quantum information tasks.

The quantum control of these kinds of systems can be implemented using pulses of external fields. This issue is of great importance in quantum computation and a future work about the interaction of electromagnetic fields with the system presented here is in progress. Of course the decoherence, not considered in these works, plays a very important role in the quantum dynamics of these kinds of devices. Studies in Markovian scenarios suggested that the entanglement vanishes due to decoherence, while the decoherence process in non-Markovian regimes sometimes gives rise to an interesting new

J. Phys. B: At. Mol. Opt. Phys. **46** (2013) 065501

D S Acosta Coden *et al*

effect: entanglement sudden revival [19, 43–45]. We think that it is very interesting and useful to study the non-Markovian dynamics of these systems in the low and high entanglement regions depicted in this paper.

Acknowledgments

References

[1] van der Wiel W G, De Franceschi S, Elzerman J M, Fujisawa T, Tarucha S and Kouwenhoven L P 2003 *Rev. Mod. Phys.* **75** 1
Hanson R, Kouwenhoven L P, Petta J R, Tarucha S and Vandersypen L M K 2007 *Rev. Mod. Phys.* **79** 1217
Lee S J, Souma S, Ihm G and Chang K J 2004 *Phys. Rep.* **394** 1
[2] Bastard G 1981 *Phys. Rev.* B **24** 4714
[3] Nguyen N T T and Das Sarma S 2011 *Phys. Rev.* B **83** 235322
[4] Ashoori R C, Stormer H L, Weiner J S, Pfeiffer L N, Pearton S J, Baldwin K W and West K W 1992 *Phys. Rev. Lett.* **68** 3088
[5] Wan Y, Ortiz G and Phillips P 1997 *Phys. Rev.* B **55** 5313
[6] Lee E, Puzder A, Chou M Y, Uzer T and Farrelly D 1998 *Phys. Rev.* B **57** 12281
[7] Räsänen E, Könemann J, Haug R J, Puska M J and Nieminen R M 2004 *Phys. Rev.* B **70** 115308
[8] Hu X and Das Sarma S 2000 *Phys. Rev.* A **61** 062301
[9] Sundqvist P A, Narayan V, Stafström S and Willander M 2003 *Phys. Rev.* B **67** 165330
[10] Nistor S V, Stefan M, Nistor L C, Goovaerts E and Van Tendeloo G 2010 *Phys. Rev.* B **81** 035336
[11] Narayan V and Willander M 2002 *Phys. Rev.* B **65** 125330
[12] Petta R, Johnson A C, Taylor J M, Laird E A, Yacoby A, Lukin M D, Marcus C M, Hanson M P and Gossard A C 2005 *Science* **309** 2180
[13] Schlosshauer M 2005 *Rev. Mod. Phys.* **76** 1267
[14] Bennett C H 1995 *Phys. Today* **48** 24
[15] Xu J, Xu X, Li C, Zhang C, Zou X and Guo G 2010 *Nature Commun.* **1** 7
[16] Yu T and Eberly J H 2002 *Phys. Rev.* B **66** 193306
[17] Ferrón A, Domínguez D and Sánchez M J 2012 *Phys. Rev. Lett.* **109** 237005
[18] Álvarez G A and Suter D 2010 *Phys. Rev. Lett.* **104** 230403
[19] Majtey A P and Plastino A R 2012 *Int. J. Quantum Inform.* **10** 1250063
[20] Tichy M, Mintert F and Buchleinter A 2011 *J. Phys. B: At. Mol. Opt. Phys.* **44** 192001
[21] Amico L, Fazio L, Osterloh A and Vedral V 2008 *Rev. Mod. Phys.* **80** 517
[22] Abdullah S, Coe J P and DAmico I 2009 *Phys. Rev.* B **80** 235302
[23] He L and Zunger A 2007 *Phys. Rev.* B **75** 075330
[24] He L, Bester G and Zunger A 2005 *Phys. Rev.* B **72** 195307
[25] Coe J P and DAmico I 2010 *J. Phys.: Conf. Ser.* **254** 012010
[26] Coe J P, Sudbery A and DAmico I 2008 *Phys. Rev.* B **77** 205122
[27] Osenda O and Serra P 2007 *Phys. Rev.* A **75** 042331
[28] Osenda O and Serra P 2008 *J. Phys. B: At. Mol. Opt. Phys.* **41** 065502
[29] Ferrón A, Osenda O and Serra P 2009 *Phys. Rev.* A **79** 032509
[30] Pont F M, Osenda O, Toloza J H and Serra P 2010 *Phys. Rev.* A **81** 042518
[31] Pont F M, Osenda O and Serra P 2010 *Phys. Scr.* **82** 038104
[32] Majtey A P, Plastino A R and Dehesa J S 2012 *J. Phys A: Math. Theor.* **45** 115309
[33] Gondar J L and Comas F 2003 *Physica* B **322** 413
[34] Yilmaz S and Safak H 2007 *Physica* E **36** 40
[35] Özmen A, Yakar Y, Cakir B and Atav Ü 2009 *Opt. Commun.* **282** 3999
[36] Karabulut I and Baskoutas S 2008 *J. Appl. Phys* **103** 073512
[37] Sahin M 2008 *Phys. Rev.* B **77** 045317
[38] deSousa J S, Leburton J P, Freire V N and daSilva E F 2005 *Phys. Rev.* B **72** 155438
[39] Nistor V, Nistor L C, Stefan M, Mateescua C D, Birjega R, Solovieva N and Nikl M 2009 *Superlatt. Microstruct.* **46** 306
[40] Kruppa A T and Arai K 1999 *Phys. Rev.* A **59** 3556
[41] Acosta Coden D S, Gomez S S and Romero R H 2011 *J. Phys. B: At. Mol. Opt. Phys.* **44** 035003
[42] Gomez S S and Romero R H 2009 *Cent. Eur. J. Phys.* **7** 12
[43] Bellomo B, Lo Franco R and Compagno G 2007 *Phys. Rev. Lett.* **99** 160502
[44] Yu T and Eberly J H 2009 *Science* **323** 598
[45] Lastra F, Reyes S A and Wallentowitz S 2011 *J. Phys. B: At. Mol. Opt. Phys.* **44** 015504